SCIENCE CHINA
Technological Sciences

•Article•

May 2022 Vol.65 No.5: 1169–1178
https://doi.org/10.1007/s11431-021-1993-9

Porous fiber paper and 3D patterned electrodes composed high-sensitivity flexible piezoresistive sensor for physiological signal monitoring

HOU XiaoJuan[1], ZHONG JiXin[1], HE Jian[1*], YANG ChangJun[1], YU JunBin[1], MEI LinYu[2], MU JiLiang[1], GENG WenPing[1] & CHOU XiuJian[1]

[1] *Science and Technology on Electronic Test and Measurement Laboratory, North University of China, Taiyuan 030051, China;*
[2] *School of Mechanical Engineering, North University of China, Taiyuan 030051, China*

Received October 11, 2021; accepted December 29, 2021; published online February 28, 2022

The research on flexible pressure sensors has drawn widespread attention in recent years, especially in the fields of health care and intelligent robots. In practical applications, the sensitivity of sensors directly affects the precision and integrity of weak pressure signals. Here, a pressure sensor with high sensitivity and a wide measurement range composed of porous fiber paper and 3D patterned electrodes is proposed. Multi-walled carbon nanotubes with excellent conductivity were evenly sprayed on the fiber paper to form the natural spatial conducting networks, while the copper-deposited polydimethylsiloxane films with micro-pyramids array were used as electrodes and flexible substrates. Increased conducting paths between electrodes and fibers can be obtained when high-density micro-pyramids fall into the porous structures of the fiber paper under external pressure, thereby promoting the pressure sensor to show an ultra-high sensitivity of 17.65 kPa^{-1} in the pressure range of 0–2 kPa, 16 times that of the device without patterned electrodes. Besides, the sensor retains a high sensitivity of 2.06 kPa^{-1} in an ultra-wide measurement range of 150 kPa. Moreover, the sensor can detect various physiological signals, including pulse and voice, while attached to the human skin. This work provides a novel strategy to significantly improve the sensitivity and measurement range of flexible pressure sensors, as well as demonstrates attractive applications in physiological signal monitoring.

flexible pressure sensor, high sensitivity, wide measurement range, fiber paper, 3D patterned electrodes, physiological signal monitoring

Citation: Hou X J, Zhong J X, He J, et al. Porous fiber paper and 3D patterned electrodes composed high-sensitivity flexible piezoresistive sensor for physiological signal monitoring. Sci China Tech Sci, 2022, 65: 1169–1178, https://doi.org/10.1007/s11431-021-1993-9

1 Introduction

With the rapid development of flexible electronic technology, flexible pressure sensors have demonstrated attractive applications in the field of intelligent healthcare [1–3]. Monitoring of physiological signals closely related to human health, including pulse and heart rates, has drawn growing attention among researchers and is also regarded as an important index for the performance evaluation of pressure sensors [4]. For the undistorted detection of these weak and diverse signals, both high sensitivity and wide linear regions are required. Highly sensitive flexible pressure sensors based on the piezoresistive effect [5–8], piezoelectric effect [9–12], triboelectric effect [13–16], and capacitance effect [17–20] have been developed in recent years. Among these, piezoresistive sensors, typical sensors transducing pressure into the resistance signal, have been widely used in wearable devices for a lot of advantages, including cost-efficient fabrication, simple structure, and easy process [21,22].

Numerous methods have been developed for fabricating

*Corresponding author (email: drhejian@nuc.edu.cn)

flexible piezoresistive sensors with high sensing performance, such as the employment of ultra-elastic substrates, porous conducting networks, and patterned electrodes. Traditional polymer materials, including hydrogel [23], polydimethylsiloxane (PDMS) [24], and Ecoflex [25], are considered excellent elastic substrates because of their low Young's modulus and strong chemical stability [26]. Elastic conducting composites with piezoresistive properties can be obtained by blending conductive materials such as metal nanoparticles [27], nanowires [28], graphene [29], and carbon nanotubes (CNTs) [30]. However, due to the strong Van der Waals force, the micro-nano scale conductive particles are inclined to agglomerate in flexible substrates [31], thereby resulting in inferior sensitivity and limited applications. Numerous methods have been proposed to efficiently improve the sensitivity and measurement range, such as employing porous spatial conducting framework including foam [32–34] and fiber paper [35–40]. This type of pressure sensor demonstrates enhanced sensitivity in monitoring physiological signals including pulse and voice. However, the applicative pressure range of high sensitivity is limited due to the single mechanism of resistance variation originating from the connection among conducting particles. Even though novel two-dimension multi-layer conducting materials, such as MXene [41,42] can significantly enhance the range of high sensitivity by forming extra conducting paths between interlayers under larger stress [43,44], the high costs of raw materials and synthetic method impede its widespread applications. Thus, the development of more effective methods to improve the sensitivity and measurement range remains an attractive project for researchers. To date, few reports have focused on the contact behavior between the surface of the flexible porous conducting framework and electrodes under external pressure. In addition to the inherent conductive networks of porous materials, changes in the contact area between patterned electrodes and sensitive layers will also cause significant changes in resistance, thereby affecting the performance of piezoresistive sensors, such as sensitivity, measurement range, and response time [45].

In this work, a pressure sensor with high sensitivity and ultrawide measurement range based on porous fiber paper and 3D patterned electrodes has been proposed. Multi-walled CNTs (MWCNTs) with excellent conducting properties were evenly sprayed on the surface of fiber paper to form the sensitive material, and the Cu-deposited PDMS films with 3D micro-pyramid array structure constitute the top and bottom electrode. The geometrical shapes of the micro-pyramid and CNT content significantly influence the sensing performance, which has been quantitatively studied. With 1.5% CNT content and a standard pyramid structure, the obtained pressure sensor exhibits an ultra-high sensitivity, reaching 17.65 kPa^{-1} in the pressure range of 0 to 2 kPa and 2.06 kPa^{-1} in the pressure range of 2 to 150 kPa, ~16 times higher than that of the device without microstructure. The excellent performance is mainly ascribed to the coupled effect of the porous structure of the fiber paper and hump-electrodes: the pyramids can fall into the interior of the fiber paper under external pressure and contact more fibers, thereby facilitating the formation of conducting paths. Based on the excellent sensing performance, the pressure sensor achieves the detection of wrist pulse, voice variation, and finger motion when attached to human skin, sufficiently meeting the requirements of practicability.

2 Experimental section

2.1 Fabrication of wafers with micro-pyramid structure

The micropattern on the mask (67 μm×67 μm) was transferred to a 4-inch Si wafer with a 500 nm-thickness SiO_2 layer using photolithography. Then, the exposed wafer was immersed in the BOE solution at 80°C for 5 min to etch the SiO_2 layer. Subsequently, the Si layer was etched by immersing in the TMAH solution at 80°C for 40 min, 30 min, and 20 min to obtain the micro-pyramid arrays and different micro-frustum array structures. The information on raw materials is provided in our previous work [46,47].

2.2 Preparation of flexible 3D-patterned electrodes

The PDMS matrix and curing agent (Dow Corning Sylgard 184) were fully mixed at a mass ratio of 10:1 for 15 min by mechanical stirring. Next, the mixture was kept in a vacuum box for 30 min to completely remove the bubbles. Subsequently, the PDMS mixture was spin-coated onto a silicon wafer with high-density inverted micro-pyramids at 900 rpm for 20 s and solidified at 90°C for 15 min. Then, the copper was deposited on the PDMS film by magnetron sputtering instrument (DENTON VACUUM Explorer) (thickness: 200 nm, sputtering time: 6 min). Finally, PDMS films with two different sizes (1.2 cm×1.2 cm and 1.0 cm×1.0 cm) were fabricated by cutting.

2.3 Preparation of MWCNT/Paper film

First, MWCNTs (0.15 g, Nanjing Xianfeng Nanotechnology Co., Ltd.) and polyvinyl pyrrolidone (PVP K30, 0.05 g, Sinopharm Chemical Reagent Co., Ltd.) were dispersed in deionized (DI) water (9.8 g) to prepare a 1.5%-concentrate MWCNT solution, followed by ultrasonic dispersion for 40 min. Then, the well-dispersed MWCNT solution was uniformly sprayed on the two sides of fiber paper (10 cm× 10 cm) by an electric sprayer. Next, the paper-based MWCNT film was placed on the drying table (LabTe-

chEH20B) at 70°C for 5 min. Finally, samples with a size of 1 cm×1 cm were cut from the peeled PMC film.

2.4 Assembling the pressure sensor

The PDMS electrodes were placed on top and underneath the PMC film to form a sandwich structure. Then, the sensor was protected on both sides with Kapton tapes.

2.5 Characterization and measurement

The morphology of the material surface was investigated by a scanning electron microscope (SEM) (HITACHI-SU8010). The Raman and X-ray diffraction (XRD) spectra of MWCNTs were obtained using a Raman spectrometer (Renishaw inVia laser at 532 nm) and X-ray diffractometer (Cu-K radiation). The constant voltage (1 V) was applied by a DC Power supply (UTP3313TFL-II). The current was measured by an electrometer (Keithley 2611B). The compression test was performed by a tensile strength tester (GOTECH-AI-3000S).

3 Results and discussion

Figure 1(a) illustrates the manufacturing process of the pressure sensor. First, MWCNT/PVP solution dispersed via ultrasonic treatment with high stability and no hierarchy after 24 h (Figure 1(b)) was evenly sprayed on a fiber paper by electric spraying to form a paper/MWCNT (PMC) film. Subsequently, the mixture of PDMS and the cross-linking agent was poured onto the silicon wafer with high-density pyramids; a flexible PDMS electrode with a 3D patterned structure was obtained by curing, peeling, and copper sputtering. To assemble the pressure sensor, the PMC film was placed between the top and bottom layers of the Cu-deposited micro-pyramid PDMS film and then protected by Kapton tapes. The assembled sandwich structured sensor is shown in Figure 1(c).

Figure 2(a)–(b) presents the morphologies of the 3D patterned PDMS film characterized by SEM. Uniform formation of high-density micro-pyramid array structure is observed on the surface of PDMS film. The corresponding length of the bottom sides and the total height of a single pyramid are ~67 μm and ~50 μm (shown in Figure 2(c)), respectively. As Figure 2(d) shows, the fiber paper (thickness: 0.3 mm) consists of spatially interlaced fibers with an average diameter of 11.42 μm (Figure S1 Supporting information), which can easily contact each other and form conducting network under external pressure. Besides, the porous structure promotes the 3D pyramids to fall into the interior of fiber paper and contact more conducting fibers. Figure 2(e)–(g) depicts the SEM images of the PMC film with different scale bars, revealing that the MWCNTs are

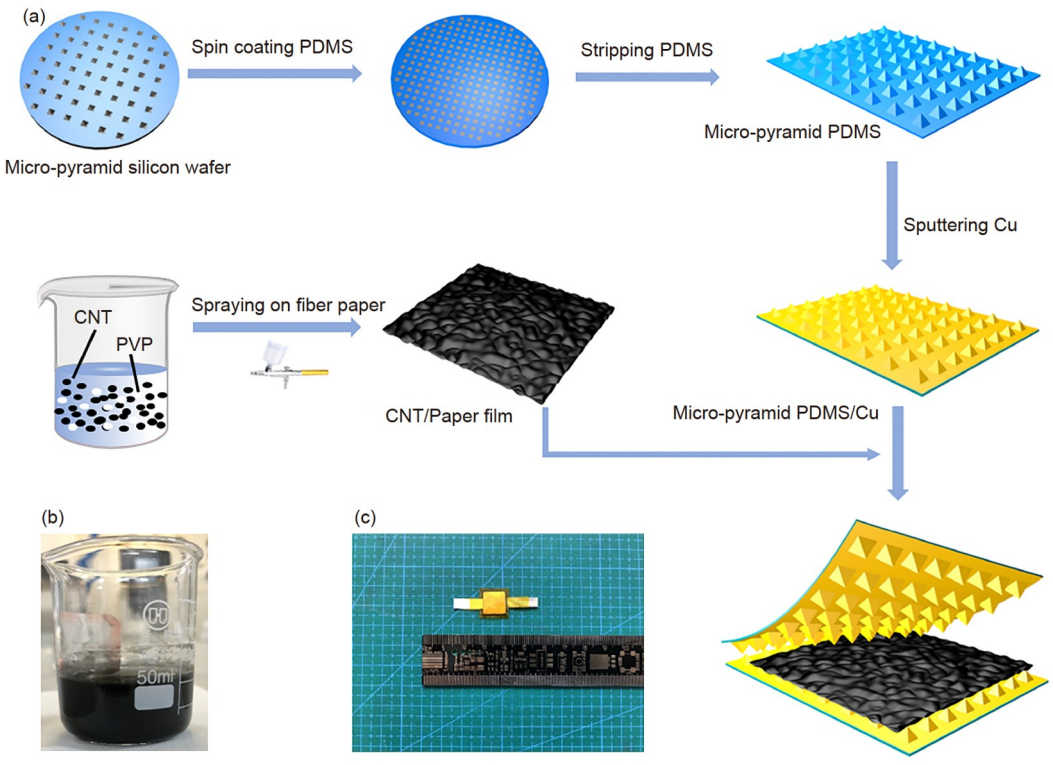

Figure 1 (Color online) Fabrication and structure of the piezoresistive sensor. (a) Fabrication process of the flexible micro-pyramid array electrode and Paper/MWCNTs film. (b) MWCNT solution after remaining in the air for 24 h. (c) Fabricated pressure sensor.

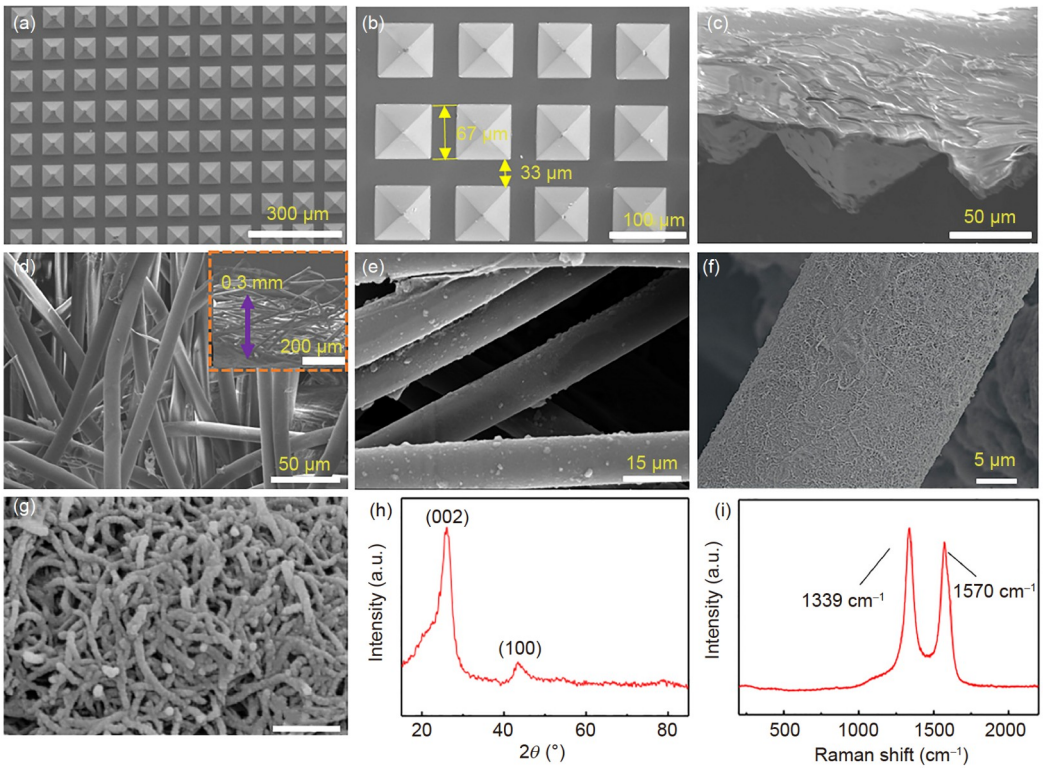

Figure 2 (Color online) Characterization analyses of the 3D patterned structure, paper, and MWCNTs. (a)–(c) SEM images of the Cu-deposited micro-pyramid array film. (d) SEM image of the fiber paper surface (inset: cross section). (e)–(g) SEM images of the paper/MWCNT film. (h) XRD and (i) Raman figures of the MWCNT powders.

evenly dispersed on the fiber surfaces without serious agglomeration. The average thickness (~0.5 μm) of a CNT film is calculated by measuring the average diameter of CNT-attached fibers (Figure S1). XRD and Raman spectrum analyses were performed to characterize the MWCNT composition, as displayed in Figure 2(h)–(i). The sharp diffraction peak of MWCNTs at around 26° (Figure 2(h)) reflects high crystallinity, contributing to the high conductivity. Besides, two sharp Raman characteristic peaks at around 1339 cm^{-1} and 1570 cm^{-1} are observed in Figure 2(i), attributed to the scattering of amorphous carbon and integrity of the sp^2 hybrid bond structures, respectively.

The sensing mechanism of the pressure sensor is illustrated in Figure 3. As Figure 3(a) shows, the total resistance of the pressure sensor comprises the contact resistance (R_C) between the PMC film and micro-pyramid-structured electrodes, the self-resistance of the metal electrodes (R_M), and alterable resistance of the PMC film (R_P). The compression strain test was performed under different pressures to investigate the compressing deformation difference between the PMC and PDMS film (Figure 3(b)). The fiber paper generated larger deformation than PDMS under arbitrarily applied pressure due to the spatial porous structure, implying that the change in R_P will dominate the total resistance. The dynamic model can be illustrated as follows: at the initial state, the interface between the PMC film and micro-pyramids array electrodes shows a larger resistance compared with the PMC film itself. Under low pressure (Figure 3(c)), the porous interior (inset of Figure 2(d))-induced high compressibility facilitates the connection of the conducting fibers, greatly increasing the conductivity. Simultaneously, the micro-pyramids move toward the fiber paper interior through the pores and contact more conducting fibers, thereby decreasing the contact resistance. With the continuous increase in the external pressure, the fiber paper exhibits a slower linear stress-strain behavior (Figure 3(b)) due to the growing elastic force originating from the compressed fibers, with a gentle R_P variation. Significantly, the micro-pyramids fallen into the paper generate significant deformation (42 μm at 150 kPa, ~85% of the micro-pyramid height) and encourage more contact points between the electrodes and the paper fibers (Figure 3(d)), inducing the increase in R_C. The alterable resistance of the pressure sensor can be expressed as follows:

$$R_P = R_{P1} // R_{P2} \cdots // R_{Pn}, \tag{1}$$

$$R_C = R_{C1} // R_{C2} \cdots // R_{Cn}, \tag{2}$$

$$R_{Ci} = \rho_C \frac{1}{S}, \tag{3}$$

where ρ_C is the coefficient of the contact resistance, S is the contact area between a single micro-pyramid and the PMC film. Therefore, the total resistance (R_T) of the sensor can be

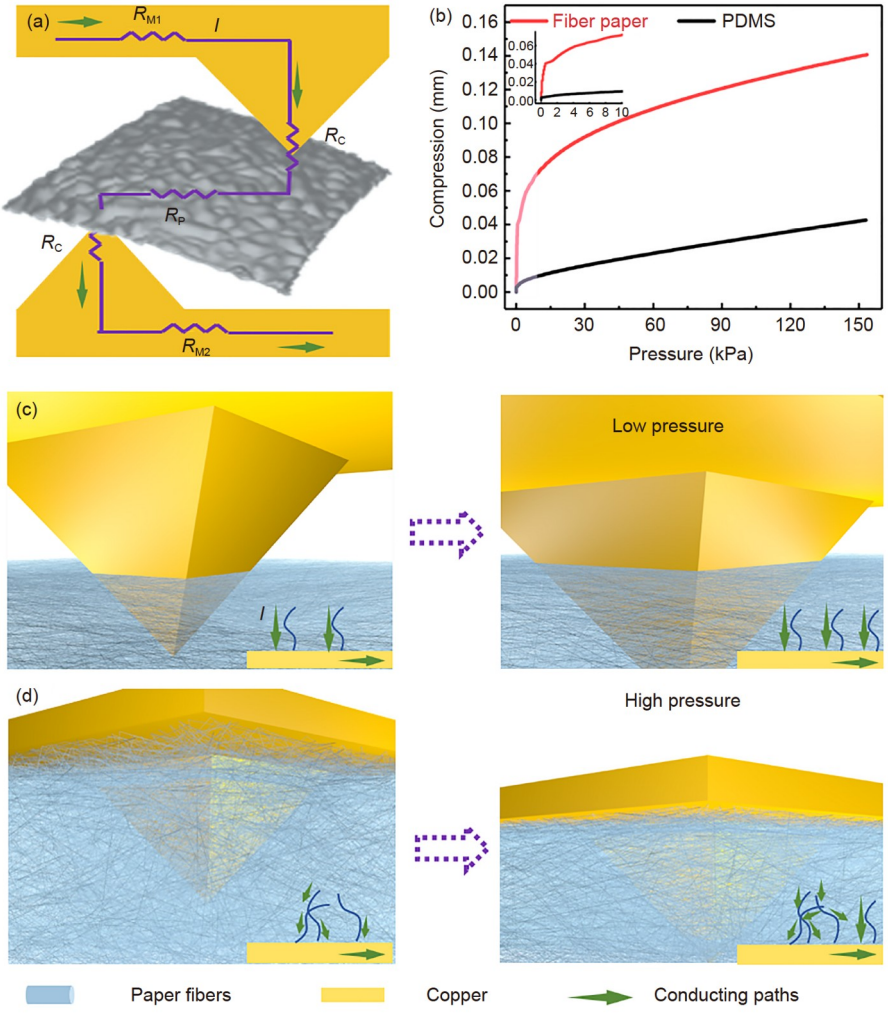

Figure 3 (Color online) Sensing mechanism of the pressure sensor. (a) Schematic resistance network of the pressure sensor. (b) Compression curves of the PDMS film and the fiber paper. Real-time state of the sensor under (c) low pressure and (d) high pressure.

expressed as follows:

$$R_T = R_M + R_P + R_C. \tag{4}$$

When a constant voltage is supplied to the sensor by a regulated DC power supply, the current I flows through the apex of pyramid-like microstructure to the PMC film, varying with the contact resistance. As a vital performance index, the sensitivity (S) of the sensor can be defined as follows:

$$S = \frac{I - I_0}{I_0 \Delta P} = \frac{\Delta I}{I_0} \times \frac{1}{\Delta P}, \tag{5}$$

where I_0 is the initial current without external pressure and ΔP is the pressure variation.

To study the effect of patterned structure on the sensing performance, three kinds of pyramid-like structures, named Pyramid, Frustum 1, and Frustum 2 according to the height of the truncated small pyramid, were constructed, as shown in Figure 4(a)–(c) and Figure S2. The stress distribution of the three kinds of structures under vertical pressure was simulated using the COMSOL software, and the corresponding sensitivity was acquired simultaneously. As shown in Figure 4(d), the electrode with pyramid structures applies the highest stress on the fiber paper surface under a consistent pressure (0.4 kPa). Besides, the generated strain on the fiber paper increases as the micro-pyramid height decreases, which is identical to the simulated sensitivity curve, as shown in Figure 4(e).

To investigate the practical performance difference between sensors containing the structured and non-structured electrodes, three pressure sensors were fabricated with different pyramid-like array electrodes. Figure 4(g) presents the measured current curves, from which it is observed the pyramid electrode-based sensor generates the highest valve of $\Delta I/I$. Moreover, the $\Delta I/I$ declined with the decrease in the pyramid height, verifying the stress-induced performance enhancement of the 3D pyramid structure. Significantly, the $\Delta I/I$ valve was much higher than the simulated valve, mainly ascribed to the porous structure of the fiber paper and the

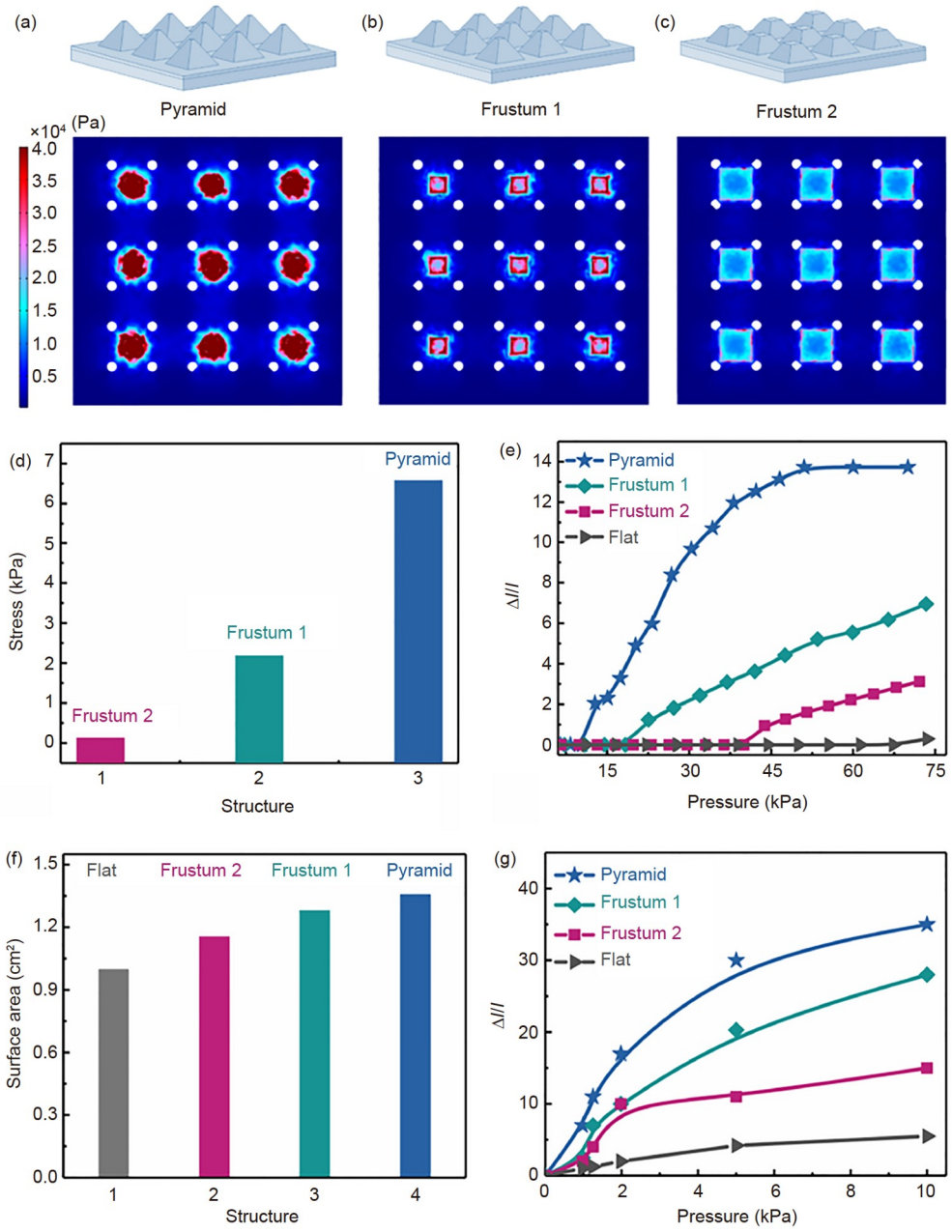

Figure 4 (Color online) Measurement and simulation of the pressure sensors with different structures. (a)–(c) Diagrams and stress distributions of the different structures. (d) Average stress of the different patterned structures. (e) Simulated current variation curves. (f) Calculated surface areas of the micro-structured electrodes. (g) Measured current variation curves.

dynamic process of the pyramids falling into the pores between the fibers. In addition, the surface area is a key factor for that a larger surface area contributes to more contact points between the conducting paper fibers and electrodes. The theoretical surface areas of the three structured electrodes (1 cm×1 cm) were calculated by the following formula:

$$S_{\mathrm{A}} = 1 + n(b^2 - a^2) + 4na\frac{\sqrt{\left(\frac{a}{2}\right)^2 + h^2}}{2}\left(1 - \frac{b^2}{a^2}\right), \tag{6}$$

where n is the number of pyramids, a is the length of the bottom side, b is the length of the topside, and h is the pyramid height. As shown in Figure 2(b) and Figure S3, the top sides of the Pyramid, Frustum 1, and Frustum 2 are 0, ~30, and ~50 μm, respectively. From eq. (6), the pyramid structure shows the highest surface area, enhanced by 34% compared to the electrode without any structure (Figure 4 (f)).

Figure 5(a) presents the current variation curves of the pressure sensor under CNT concentrations varying from 0.5% to 2% under the external pressure of 10 kPa. The valve

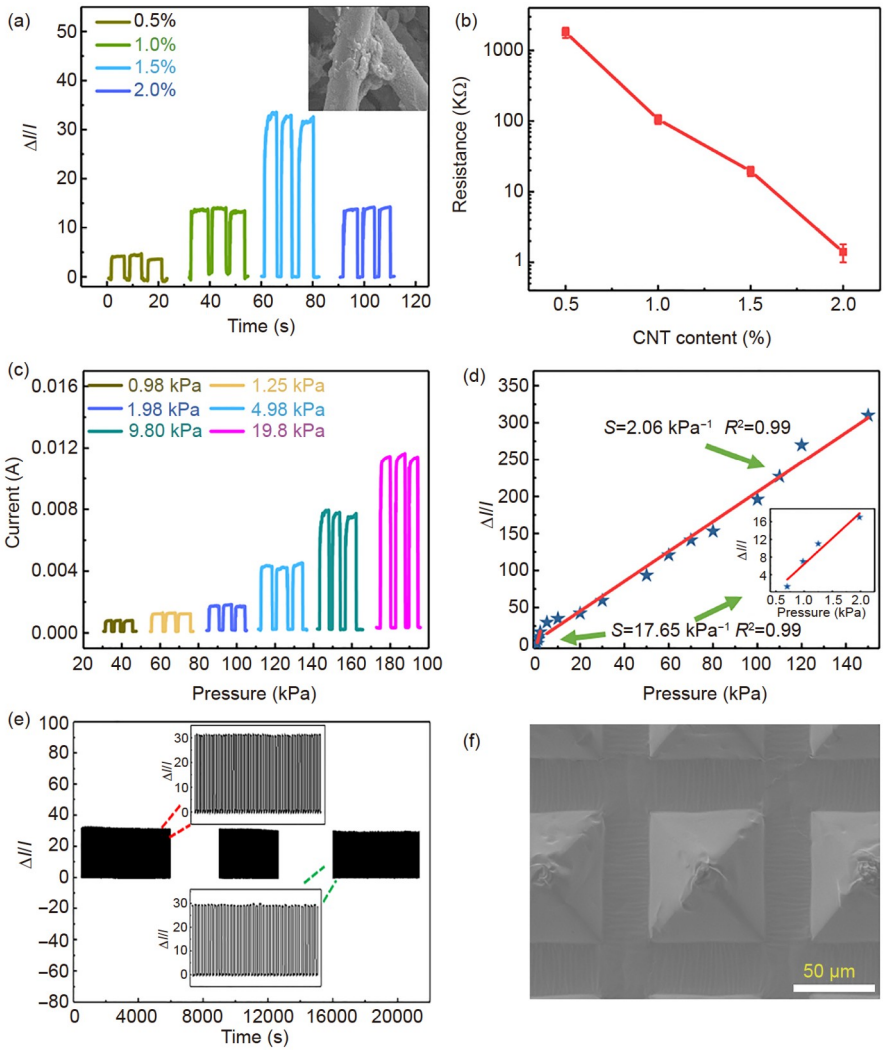

Figure 5 (Color online) Sensing performance of the pressure sensor. (a) Current variation curves of the pressure sensor under different MWCNT concentrations. (b) Surface of the conducting fiber paper with different CNT contents. (c) Current curves of the pressure sensor under different external pressures. (d) Fitted pressure sensitivity curve. (e) Current variation curve of the pressure sensor for 20,000 cycles. (f) SEM image of the micro-pyramid array structure after the cycle test.

of $\Delta I/I$ shows a growing tendency from 0.5% to 1.5%, ascribed to more MWCNTs attaching to the surface of the paper fibers and tends to decrease as the MWCNT concentration increases. This is because the MWCNT content on paper fibers reached the saturation point at the concentrate of 1.5%. Although the continuous increase in the MWCNT content improves the conductivity of PCM film (reflected by the decreasing surface resistance shown in Figure 5(b)), paper fibers with small gaps can contact each other through the MWCNTs (inset of Figure 5(a)), resulting in a smaller variation of conducting paths under the same external pressure, thereby affecting the current variation. As Figure 5(c) illustrates, the pressure sensor exhibits high resistance variation when the pressure is altered widely from 0.98 to 19.8 kPa. Figure 5(d) shows the $\Delta I/I$–ΔP curves of the pressure sensor constructed with the micro-pyramid array electrode. After piecewise linear fitting, two curve segments based on the slope are observed. In the pressure range of 0–2 kPa, the pressure sensor displays an ultra-high sensitivity of 17.65 kPa^{-1} due to the superimposed effect of increasing contact area originated from the 3D patterned structure falling into fiber paper, and a sensitivity of 2.06 kPa^{-1} in the pressure range of 2–150 kPa, superior to most of the previously reported paper-based sensors, listed in Table 1. To investigate the performance stability, the current variation of the device is measured by a homemade motor system (Figure S4) under a repeated 1 N load/unload force for more than 20,000 cycles. The initial and final waveforms of the current response showed almost the same results, as shown in Figure 5(e), revealing that the pressure sensor exhibits high repeatability, stability, and durability. The SEM image of the micro-pyramid array electrode after the cycle test is presented in Figure 5(f), wherein the micro-patterns and the sharp peaks remain intact after long-term compres-

sion, demonstrating favorable mechanical stability. Simultaneously, a response time of 75 ms was obtained, as shown in Figure S5.

In view of the excellent sensitivity of the as-fabricated sensor at a low-pressure stage, we applied the sensor to practical physiological signal detection. Figure 6(a) shows

Table 1 Summary of partial highly-sensitive piezoresistive sensors

Flexible framework	Conducting filler	Electrodes	Sensitivity (kPa^{-1})	Linear region (kPa)	Minimum detection (Pa)	References
Cotton fabric	MXene	Interdigital electrodes	5.3	1.3	/	[34]
Aerogels	MXene/rGO	Planar	0.28	66.98	60	[48]
Porous PGS	CNTs	Planar	8	8	100	[49]
PU foam	CNF&CB	Planar	0.35	2.2	/	[33]
PDMS/nickel foam	Graphene	Planar	5.37	1	4.4	[32]
Silicon Rubber	CNTs	/	0.096	175	/	[50]
Cotton fabric	CNTs	/	12.96	0.1	10	[51]
Tissue paper	Au nanowires	Interdigital electrodes	1.14	50	13	[52]
Tissue paper	Polypyrrole	Printing Paper/PPy	4.8	5.5	350	[53]
Paper	Carbonization	Interdigital electrodes	2.56–5.67	2.53	0.9	[54]
Fiber paper	CNTs	3D patterned electrodes	17.65 2.06	2 150	18	This work

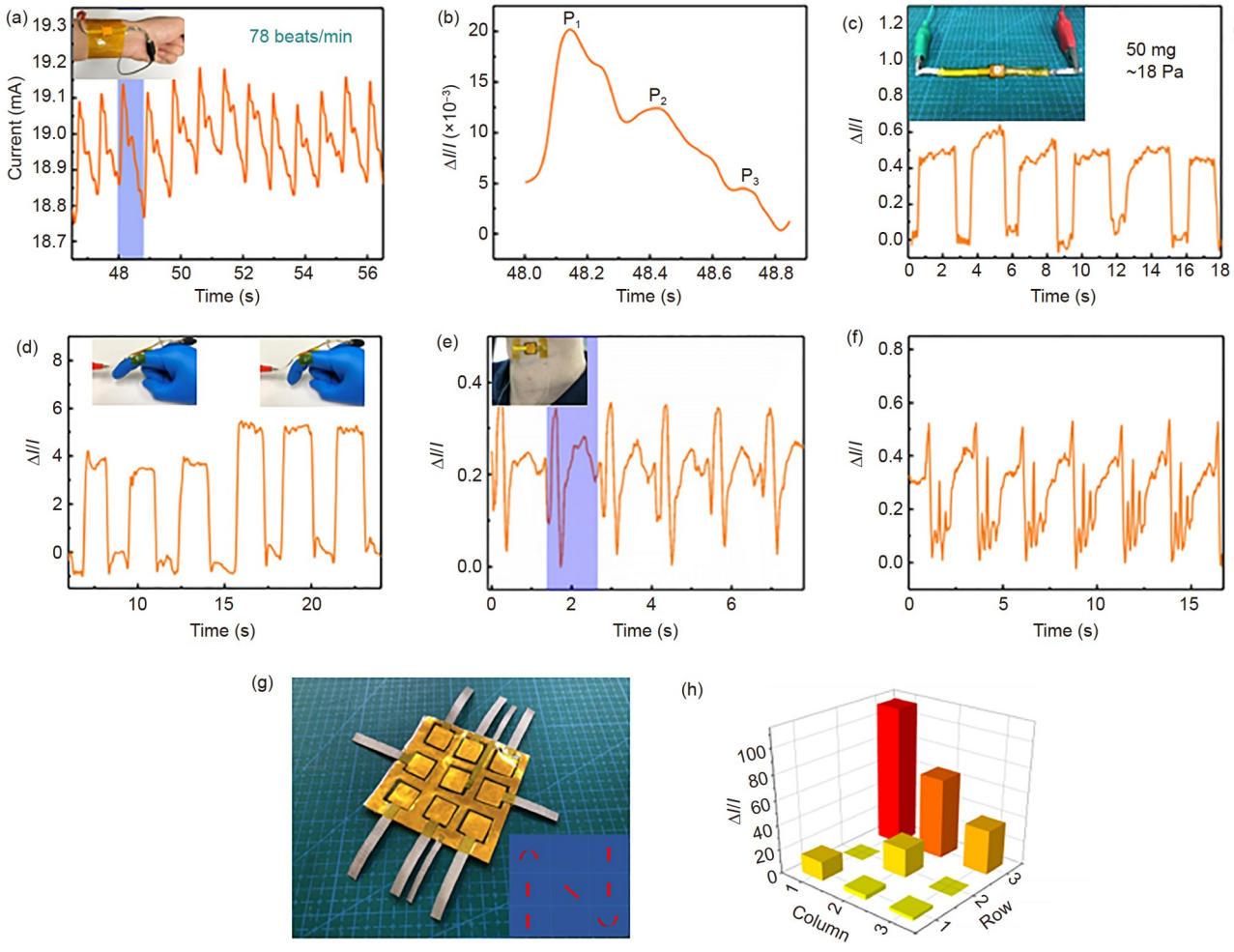

Figure 6 (Color online) Tactile signal detection applications of the pressure sensor. (a) Record of the pulse wave. (b) Amplified pulse waveform of (a). (c) Current variation of the pressure sensor under the repeat stimulation of an M4 nut. (d) Current variation of the pressure sensor attached on a finger at different bending degrees. (e), (f) Waveforms generated when saying different words. (g) Picture of a sensor array. (h) Pressure distribution when writing the letter "N" on the sensor.

the wrist pulse signals of a healthy human wearing the high-sensitivity pressure sensor. According to the schematic, it is easy to accurately count the pulse (78 beats/min). Figure 6(b) presents a single pulse consisting of three wave peaks: the first systolic peak pressure (P_1), the second systolic peak pressure (P_2), and the diastolic wave (P_3) [55], related to human health status. Through qualitative analysis of the pulse wave, some key parameters can be derived to evaluate health conditions, such as the radical Augmentation Index (AI), which is regarded as an index for evaluating vascular aging [56]. Figure 6(c) shows that the pressure sensor can steadily and sensitively detect the pressure of a Teflon nut weighing about 50 mg (18 Pa). The pressure sensor can also fit the finger and measure its curvature, as shown in Figure 6 (d). Besides, the voice variation signals can also be detected. Figure 6(e)–(f) respectively show the current variation curves when repeatedly saying "pressure sensor" and "carbon", revealing that different voice signals are significantly translated into corresponding current signals by the piezoresistive sensor. To expand the application of the sensor in large-area pressure detection, a pressure sensor array is fabricated based on the single flexible pressure sensor, as shown in Figure 6(g). The pressure sensor array contains 3×3 pixels and a 5 cm×5 cm testing area. As shown in Figure 6(h), the pressure sensor array can output distinguishable current variation signals reflecting the pressure distribution when writing the letter "N" on it with different forces, thereby showing favorable potential in the field of E-skin.

4 Conclusions

In summary, a piezoresistive sensor with ultra-high sensitivity and a wide measurement range based on porous fiber paper and 3D patterned electrodes has been proposed. By optimizing the initial resistance of the conducting paper and the shape of the 3D pattern, the pressure sensor exhibits an ultra-high sensitivity of 17.65 kPa^{-1} in the external pressure range of 0 to 2 kPa and retains a sensitivity of 2.06 kPa^{-1} in a measuring range of 150 kPa. The enhanced performance is mainly ascribed to the couple effect of 3D patterned electrodes and porous sensitive layer. On the one hand, the 3D pyramid structure effectively enhances the surface area of electrodes, equivalent to the sensing nodes. On the other hand, the inverted pyramid can easily fall into the interior of the fiber paper through the pores, significantly facilitating the formation of numerous conducting paths and improving the current response. Additionally, the pressure sensor exhibits remarkable mechanical stability with a stable current response after 20,000 cycling tests. Based on the improved sensing performances, the pressure sensor achieves undistorted signal detection, including weak pulse, voice, and joint movements while attached to the human skin. This work presents a novel strategy for significantly improving the sensitivity and measurement range of flexible piezoresistive sensors and demonstrates the applications with favorable prospects in intelligent healthcare.

This work was supported by the National Key R&D Program of China (Grant Nos. 2019YFE0120300, 2019YFF0301802), National Natural Science Foundation of China (Grant Nos. 52175554, 62101513, 51975542), Natural Science Foundation of Shanxi Province (Grant No. 201801D121152), Shanxi "1331 Project" Key Subject Construction (Grant No. 1331KSC), National Defense Fundamental Research Project, and Research Project Supported by ShanXi Scholarship Council of China (Grant No. 2020-109).

Supporting Information

The supporting information is available online at tech.scichina.com and link.springer.com. The supporting materials are published as submitted, without typesetting or editing. The responsibility for scientific accuracy and content remains entirely with the authors.

1 Chen S, Qi J, Fan S, et al. Flexible wearable sensors for cardiovascular health monitoring. Adv Healthc Mater, 2021, 10: 2100116
2 Guo Y, Wei X, Gao S, et al. Recent advances in carbon material-based multifunctional sensors and their applications in electronic skin systems. Adv Funct Mater, 2021, 31: 2104288
3 Shao J Y, Chen X L, Li X M, et al. Nanoimprint lithography for the manufacturing of flexible electronics. Sci China Tech Sci, 2019, 62: 175–198
4 Li S, Xiao X, Hu J, et al. Recent advances of carbon-based flexible strain sensors in physiological signal monitoring. ACS Appl Electron Mater, 2020, 2: 2282–2300
5 Sun T, Jiang Y D, Duan Z H, et al. Wearable and washable textile-based strain sensors via a single-step, environment-friendly method. Sci China Tech Sci, 2021, 64: 441–450
6 Jiang S, Yu J, Xiao Y, et al. Ultrawide sensing range and highly sensitive flexible pressure sensor based on a percolative thin film with a knoll-like microstructured surface. ACS Appl Mater Interfaces, 2019, 11: 20500–20508
7 Li T, Chen L, Yang X, et al. A flexible pressure sensor based on an MXene-textile network structure. J Mater Chem C, 2019, 7: 1022–1027
8 Chen X, Zeng Q, Shao J, et al. Channel-crack-designed suspended sensing membrane as a fully flexible vibration sensor with high sensitivity and dynamic range. ACS Appl Mater Interfaces, 2021, 13: 34637–34647
9 Kim H J, Kim Y J. High performance flexible piezoelectric pressure sensor based on CNTs-doped 0–3 ceramic-epoxy nanocomposites. Mater Des, 2018, 151: 133–140
10 Jiang J, Tu S, Fu R, et al. Flexible piezoelectric pressure tactile sensor based on electrospun $BaTiO_3$/Poly(vinylidene fluoride) nanocomposite membrane. ACS Appl Mater Interfaces, 2020, 12: 33989–33998
11 Chamankar N, Khajavi R, Yousefi A A, et al. A flexible piezoelectric pressure sensor based on PVDF nanocomposite fibers doped with PZT particles for energy harvesting applications. Ceram Int, 2020, 46: 19669–19681
12 Chen X, Shao J, Tian H, et al. Scalable imprinting of flexible multiplexed sensor arrays with distributed piezoelectricity-enhanced micropillars for dynamic tactile sensing. Adv Mater Technol, 2020, 5: 2000046
13 Cheng Y, Wu D, Hao S, et al. Highly stretchable triboelectric tactile sensor for electronic skin. Nano Energy, 2019, 64: 103907
14 Ning C, Dong K, Cheng R, et al. Flexible and stretchable fiber-shaped triboelectric nanogenerators for biomechanical monitoring and

human-interactive sensing. Adv Funct Mater, 2021, 31: 2006679
15 Wang H L, Kuang S Y, Li H Y, et al. Large-area integrated triboelectric sensor array for wireless static and dynamic pressure detection and mapping. Small, 2020, 16: 1906352
16 Du Y, Wang X, Dai X, et al. Ultraflexible, highly efficient electromagnetic interference shielding, and self-healable triboelectric nanogenerator based on Ti_3C_2T MXene for self-powered wearable electronics. J Mater Sci Tech, 2022, 100: 1–11
17 Uzun S, Seyedin S, Stoltzfus A L, et al. Knittable and washable multifunctional MXene-coated cellulose yarns. Adv Funct Mater, 2019, 29: 1905015
18 Zhang Y, Liu S, Miao Y, et al. Highly stretchable and sensitive pressure sensor array based on icicle-shaped liquid metal film electrodes. ACS Appl Mater Interfaces, 2020, 12: 27961–27970
19 Lapčinskis L, Linarts A, Knite M, et al. Solid-state supercapacitor application for pressure sensing. Appl Surf Sci, 2019, 474: 91–96
20 Luo Y, Shao J, Chen S, et al. Flexible capacitive pressure sensor enhanced by tilted micropillar arrays. ACS Appl Mater Interfaces, 2019, 11: 17796–17803
21 Zheng Q, Lee J, Shen X, et al. Graphene-based wearable piezoresistive physical sensors. Mater Today, 2020, 36: 158–179
22 Qin J, Yin L J, Hao Y N, et al. Flexible and stretchable capacitive sensors with different microstructures. Adv Mater, 2021, 33: 2008267
23 Chang J Y, Zhang Z X, Jia F, et al. Ionic conductive hydrogels toughened by latex particles for strain sensors. Sci China Tech Sci, 2020, 64: 827–835
24 Huang Y H, Xiang Y, Ren W T, et al. Enhancing the sensitivity of crack-based strain sensor assembled by functionalized graphene for human motion detection. Sci China Tech Sci, 2021, 64: 1805–1813
25 Fortunato M, Bellagamba I, Tamburrano A, et al. Flexible ecoflex(R)/graphene nanoplatelet foams for highly sensitive low-pressure sensors. Sensors, 2020, 20: 4406
26 Tai H, Duan Z, Wang Y, et al. Paper-based sensors for gas, humidity, and strain detections: A review. ACS Appl Mater Interfaces, 2020, 12: 31037–31053
27 Schlicke H, Kunze S, Rebber M, et al. Cross-linked gold nanoparticle composite membranes as highly sensitive pressure sensors. Adv Funct Mater, 2020, 30: 2003381
28 Jeong H, Noh Y, Ko S H, et al. Flexible resistive pressure sensor with silver nanowire networks embedded in polymer using natural formation of air gap. Compos Sci Tech, 2019, 174: 50–57
29 Hao D P, Yang R X, Yi N, et al. Highly sensitive piezoresistive pressure sensors based on laser-induced graphene with molybdenum disulfide nanoparticles. Sci China Tech Sci, 2021, 64: 2408–2414
30 Sun X, Sun J, Li T, et al. Flexible tactile electronic skin sensor with 3D force detection based on porous CNTs/PDMS nanocomposites. Nano-Micro Lett, 2019, 11: 57
31 Bystrzejewski M, Huczko A, Lange H, et al. Dispersion and diameter separation of multi-wall carbon nanotubes in aqueous solutions. J Colloid Interface Sci, 2010, 345: 138–142
32 Wang J, Zhang C, Chen D, et al. Fabrication of a sensitive strain and pressure sensor from gold nanoparticle-assembled 3D-interconnected graphene microchannel-embedded PDMS. ACS Appl Mater Interfaces, 2020, 12: 51854–51863
33 Xu S, Li X, Sui G, et al. Plasma modification of PU foam for piezoresistive sensor with high sensitivity, mechanical properties and long-term stability. Chem Eng J, 2020, 381: 122666
34 Zheng Y, Yin R, Zhao Y, et al. Conductive MXene/cotton fabric based pressure sensor with both high sensitivity and wide sensing range for human motion detection and E-skin. Chem Eng J, 2021, 420: 127720
35 Li Y, Samad Y A, Taha T, et al. Highly flexible strain sensor from tissue paper for wearable electronics. ACS Sustain Chem Eng, 2016, 4: 4288–4295
36 Liu Y Q, Zhang Y L, Jiao Z Z, et al. Directly drawing high-performance capacitive sensors on copying tissues. Nanoscale, 2018, 10: 17002–17006
37 Long Y, He P, Xu R, et al. Molybdenum-carbide-graphene composites for paper-based strain and acoustic pressure sensors. Carbon, 2020, 157: 594–601
38 Tao L Q, Zhang K N, Tian H, et al. Graphene-paper pressure sensor for detecting human motions. ACS Nano, 2017, 11: 8790–8795
39 Zhu Z, Zhang H, Xia K, et al. Hand-drawn variable resistor and strain sensor on paper. Microelectron Eng, 2018, 191: 72–76
40 Wang D, Li D, Zhao M, et al. Multifunctional wearable smart device based on conductive reduced graphene oxide/polyester fabric. Appl Surf Sci, 2018, 454: 218–226
41 Cheng Y, Ma Y, Li L, et al. Bioinspired microspines for a high-performance spray $Ti_3C_2T_x$ MXene-based piezoresistive sensor. ACS Nano, 2020, 14: 2145–2155
42 Gao Y, Yan C, Huang H, et al. Microchannel-confined MXene based flexible piezoresistive multifunctional micro-force sensor. Adv Funct Mater, 2020, 30: 1909603
43 Ma Y, Liu N, Li L, et al. A highly flexible and sensitive piezoresistive sensor based on MXene with greatly changed interlayer distances. Nat Commun, 2017, 8: 1207
44 Qin R, Hu M, Li X, et al. A highly sensitive piezoresistive sensor based on MXenes and polyvinyl butyral with a wide detection limit and low power consumption. Nanoscale, 2020, 12: 17715–17724
45 Wang Z, Wang S, Zeng J, et al. High sensitivity, wearable, piezoresistive pressure sensors based on irregular microhump structures and its applications in body motion sensing. Small, 2016, 12: 3827–3836
46 Yu J, Hou X, Cui M, et al. Flexible PDMS-based triboelectric nanogenerator for instantaneous force sensing and human joint movement monitoring. Sci China Mater, 2019, 62: 1423–1432
47 Yu J, Hou X, He J, et al. Ultra-flexible and high-sensitive triboelectric nanogenerator as electronic skin for self-powered human physiological signal monitoring. Nano Energy, 2020, 69: 104437
48 Jiang D, Zhang J, Qin S, et al. Superelastic $Ti_3C_2T_x$ MXene-based hybrid aerogels for compression-resilient devices. ACS Nano, 2021, 15: 5000–5010
49 Sencadas V, Tawk C, Alici G. Environmentally friendly and biodegradable ultrasensitive piezoresistive sensors for wearable electronics applications. ACS Appl Mater Interfaces, 2020, 12: 8761–8772
50 Tang Z, Jia S, Zhou C, et al. 3D printing of highly sensitive and large-measurement-range flexible pressure sensors with a positive piezoresistive effect. ACS Appl Mater Interfaces, 2020, 12: 28669–28680
51 Ma Z, Wang W, Yu D. Highly sensitive and flexible pressure sensor prepared by simple printing used for micro motion detection. Adv Mater Interfaces, 2020, 7: 1901704
52 Gong S, Schwalb W, Wang Y, et al. A wearable and highly sensitive pressure sensor with ultrathin gold nanowires. Nat Commun, 2014, 5: 3132
53 Zhao P, Zhang R, Tong Y, et al. All-paper, all-organic, cuttable, and foldable pressure sensor with tuneable conductivity polypyrrole. Adv Electron Mater, 2020, 6: 1901426
54 Chen S, Song Y, Xu F. Flexible and highly sensitive resistive pressure sensor based on carbonized crepe paper with corrugated structure. ACS Appl Mater Interfaces, 2018, 10: 34646–34654
55 Peltokangas M, Suominen V, Vakhitov D, et al. The effect of percutaneous transluminal angioplasty of superficial femoral artery on pulse wave features. Comput Biol Med, 2018, 96: 274–282
56 Kohara K, Tabara Y, Oshiumi A, et al. Radial augmentation index: A useful and easily obtainable parameter for vascular aging. Am J Hypertension, 2005, 18: 11–14